Energy & Environmental Science

RSC Publishing

COMMUNICATION

View Article Online
View Journal | View Issue

Low-temperature processed meso-superstructured to thin-film perovskite solar cells†

Cite this: *Energy Environ. Sci.*, 2013, **6**, 1739

Received 8th March 2013
Accepted 27th March 2013

DOI: 10.1039/c3ee40810h

www.rsc.org/ees

James M. Ball, Michael M. Lee, Andrew Hey and Henry J. Snaith*

We have reduced the processing temperature of the bulk absorber layer in $CH_3NH_3PbI_{3-x}Cl_x$ perovskite solar cells from 500 to <150 °C and achieved power conversion efficiencies up to 12.3%. Remarkably, we find that devices with planar thin-film architecture, where the ambipolar perovskite transports both holes and electrons, convert the absorbed photons into collected charge with close to 100% efficiency.

Broader context

The development of photovoltaic devices which can lower the cost per unit energy of sunlight-to-electricity conversion has generally progressed along two parallel research themes: thin-film inorganic materials which exhibit high efficiency but are processed with expensive vacuum-based techniques and/or high temperature sintering; and emerging organic/hybrid materials which are readily applicable to low-cost, high-throughput, solution-based deposition procedures but suffer from a lower fundamental efficiency limit due to inherent energy losses at charge separating interfaces. Until now, no single semiconductor material has been able to combine low-temperature solution-processibility with efficient fulfilment of the three primary functions of a solar cell active layer: light absorption, free-carrier generation, and transport of both holes and electrons to their selective contacts. Here we have found that a perovskite semiconductor can accommodate all of these demanding characteristics: it can operate with the most efficient principles like an inorganic thin-film whilst maintaining the processibility of an organic semiconductor. This represents a remarkable leap forward for the development of low-cost solar cells.

Thin-film solar cells promise to reduce the cost of sunlight-to-electricity conversion compared to conventional monocrystalline silicon by using lower-cost materials and fabrication procedures. A variety of approaches have been developed with different device architectures and materials systems. Solar cells fabricated from thin-film silicon[1] and inorganic compound semiconductors[2–5] exhibit high efficiency by virtue of their ability to fulfil the multiple roles of light-absorption, charge separation, and transport of both holes and electrons in a single material. However, their fabrication procedures make use of vacuum based and/or high-temperature processing, making them relatively expensive and limited in their range of applications.[3,6] Additionally, long term pricing concerns for precursor materials may also limit the commercial success of certain systems such as CIGS and CdTe.[7] Emerging solar cell materials which can be processed with solution-based techniques at low-temperature, such as printing, should ultimately lead to the least expensive technology. Excitonic quantum dot,[8] sensitized,[9] and organic solar cells[10,11] can easily be fabricated with these deposition procedures but their maximum performance still falls short of their inorganic thin-film counterparts due to fundamental energy losses in charge separation occurring at distributed heterojunctions. Additionally, photoanodes in dye-sensitized solar cells (DSSCs) generally require sintering at 500 °C,[9] which limits substrate choice and monolithic multi-junction device architectures. For the ultimate high efficiency and low cost solar technology a semiconductor is sought which is comprised of inexpensive and abundant materials, is processable at low-temperature preferably *via* printing techniques, and generates charge freely in the bulk following light absorption, enabling low energy-loss charge generation and collection.

Semiconducting perovskites are an exciting class of materials which could fulfil these requirements. Perovskites have previously been used in nanostructured solar cells as the sensitizer,[12–14] the hole-transporter,[15] a combined sensitizer and hole-transporter,[16] and a combined absorber and electron-transporter.[17] The latter work has shown that a mixed halide perovskite absorber, $CH_3NH_3PbI_{3-x}Cl_x$, is capable of supporting electron transport when coated upon the surface of an inert scaffold in a meso-superstructured solar cell (MSSC), circumventing the significant energy losses at the electron acceptor/absorber interfaces. This allowed very high open-circuit voltages of ~1.1 V in solar cells with a perovskite bandgap of 1.55 eV.[17]

Department of Physics, University of Oxford, Clarendon Laboratory, Parks Road, Oxford, OX1 3PU, UK. E-mail: h.snaith1@physics.ox.ac.uk

† Electronic supplementary information (ESI) available: Includes supplementary methods, discussion and figures. See DOI: 10.1039/c3ee40810h

In the previous reports of perovskite-based solar cells the porous electron-transporting[12,13,16] or inert[17] metal oxides, which support and structure the absorber layer, required sintering at 500 °C. Reducing the processing temperature is important for lowering cost, enabling processing on different substrates, and processing on other device layers, in for instance multi-junction solar cells.[18] Low-temperature processable mesoporous metal oxides have been developed for DSSCs,[19–22] however, to date, the most efficient cells still require two 500 °C sintering steps.[9]

Here, we have found that Al_2O_3 nanoparticles can be deposited from a simple binder-free colloid to form the meso-superstructured scaffold with processing temperatures no higher than 150 °C. As part of this study, we investigated the influence of removing the mesoporous scaffold. With thin, porous Al_2O_3 films, a solid thin-film of the perovskite absorber is formed on top of the scaffold. This thin-film supports charge separation and transport of both carrier species with an internal quantum efficiency approaching 100% and delivers up to 9.1% power conversion efficiency in a "flat-junction" thin-film solar cell. This is the first example of a competitively efficient perovskite-based solar cell which has been shown to operate in a conventional thin-film architecture where the perovskite absorber additionally performs the tasks of charge-separation and ambipolar charge-transport of both carrier species. With the optimum Al_2O_3 film thickness we achieve power conversion efficiencies of up to 12.3% in low-temperature processed perovskite-based MSSCs.

Full details of the device fabrication and characterization are provided in the ESI.† Devices were fabricated on fluorine doped tin oxide (FTO) coated glass serving as the transparent electrode and substrate, respectively. A compact layer of TiO_2 was deposited by spin-coating from a precursor solution to act as an electron selective collection layer. The low-temperature meso-structured scaffold was deposited by spin-coating a colloidal dispersion of ~20 nm Al_2O_3 nanoparticles in isopropanol, followed by drying at 150 °C. The final thickness of the scaffold was controlled by varying the initial concentration of nanoparticles in the dispersions before spin-coating. Upon cooling to room temperature, the perovskite was deposited by spin-coating from a DMF solution of methylammonium iodide and $PbCl_2$ (3 : 1 molar ratio) which formed the perovskite after heating to 100 °C for 45 minutes. The hole-transporting material (HTM) was deposited by spin-coating a solution of 2,2′,7,7′-tetrakis-(*N*,*N*-di-*p*-methoxyphenylamine)9,9′-spirobifluorene (spiro-OMeTAD). Finally, devices were completed by evaporation of Ag electrodes through a shadow mask. Devices were measured under simulated AM 1.5, 100 mW cm^{-2} sun light with the active area defined using a metal mask to be 0.09 cm^2.

The only component in the photoactive layer of the MSSC which requires sintering is the porous alumina scaffold. By removing the polymer binder previously employed, we have managed to create uniform porous alumina films which only required drying at 150 °C. In Fig. S1† we show scanning electron microscopy (SEM) images of conventionally sintered, and low-temperature processed alumina films, which appear close to identical. Dye desorption (see ESI†) suggests that their surface areas are also similar.

To optimize devices based on the low-temperature processed alumina scaffold, we varied the thickness of this layer to assess the impact on solar cell performance. SEM images of device cross-sections incorporating "standard" 400 nm alumina scaffolds similar to the published MSSC,[17] thin 80 nm scaffolds, and devices without any mesoporous scaffold are shown in Fig. 1a–c. The perovskite coating conditions were kept constant for all scaffold thicknesses. For the thicker scaffolds, the perovskite absorber entirely infiltrates the porous alumina, coating its internal surface, as previously described.[17] The remaining porosity is filled by the p-type hole-transporter resulting in a "distributed heterojunction". For thinner alumina films, the volume of deposited perovskite exceeds the pore volume in the alumina film. A relatively thick, solid "capping layer" of perovskite is therefore formed on top of the scaffold, giving an additional stratum to the solar cell architecture. For the device with no alumina, simply a solid thin-film of perovskite is sandwiched between the n-type TiO_2 compact layer and the p-type organic HTM. In this configuration the solar cell could be described as a p–i–n heterojunction solar cell, where the intrinsic (i) layer is the perovskite absorber. The thickness of the capping layer as a function of scaffold thickness is shown in Fig. S2.† In Fig. 1d, we show a colour-enhanced SEM image of a device cross

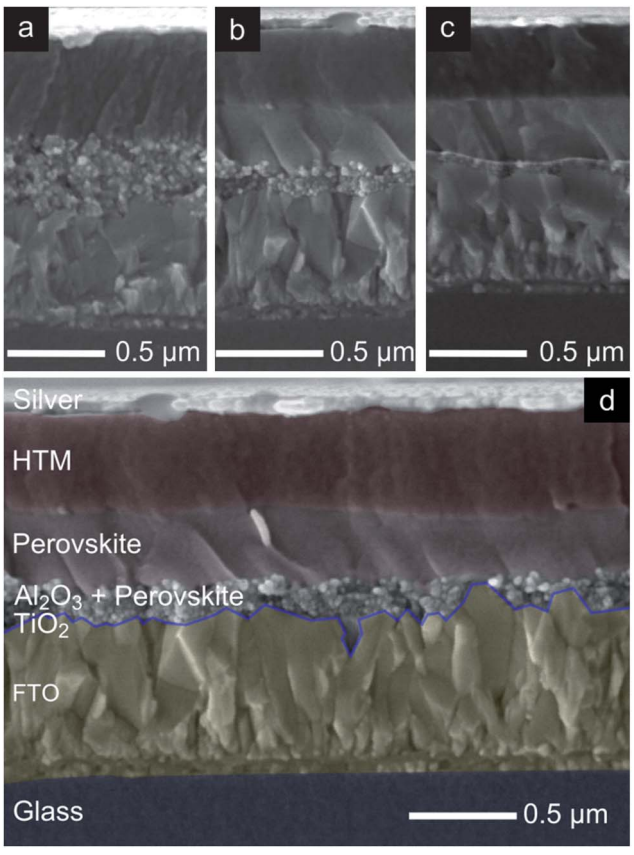

Fig. 1 Cross-sectional SEM micrographs of solar cells. Images show cells with (a) a ~400 nm thick scaffold and no perovskite capping layer, (b) a ~80 nm thick scaffold and perovskite capping layer, and (c) no scaffold. (d) Color-enhanced and annotated SEM cross-section showing a general schematic of the solar cells.

section with a thin mesoporous alumina layer, to clearly illustrate its strata.

The efficiency of a solar cell is quantified by measuring how much electrical power it generates when irradiated by standard solar illumination. The mean device parameters extracted from current–voltage curves under simulated AM 1.5, 100 mW cm^{-2} sun light, are shown in Fig. 2. A detailed summary of data for several devices, from a single batch, at each scaffold thickness are given in Fig. S5.† Starting from the thin-film p–i–n heterojunction solar cell without alumina, the photocurrent is remarkably high. The mean short-circuit current density (J_{sc}) is 13.9 ± 0.9 mA cm^{-2}, illustrating efficient charge generation and ambipolar charge-transport of both electrons and holes through the ~350 nm thick solid perovskite film. The J_{sc} increases to 16.9 ± 1.9 mA cm^{-2} for extremely thin alumina layers (~80 nm) where a thick solid perovskite film is still present, similar to the SEM image in Fig. 1d. The J_{sc} then slowly decreases with increasing alumina thickness.

To quantify the differences in generating and collecting charge more accurately, the cumulative light extinction (absorption + reflection) through the layers of the solar cells was measured. A detailed discussion of optical losses in these cells can be found in the ESI.† An example spectrum for a device with a ~400 nm scaffold is shown in Fig. 3a. By integrating the fractional light absorbed in the active layer (see Fig. S6a†) over the solar spectrum, and comparing this to the measured photocurrents, we estimate a wavelength-averaged internal

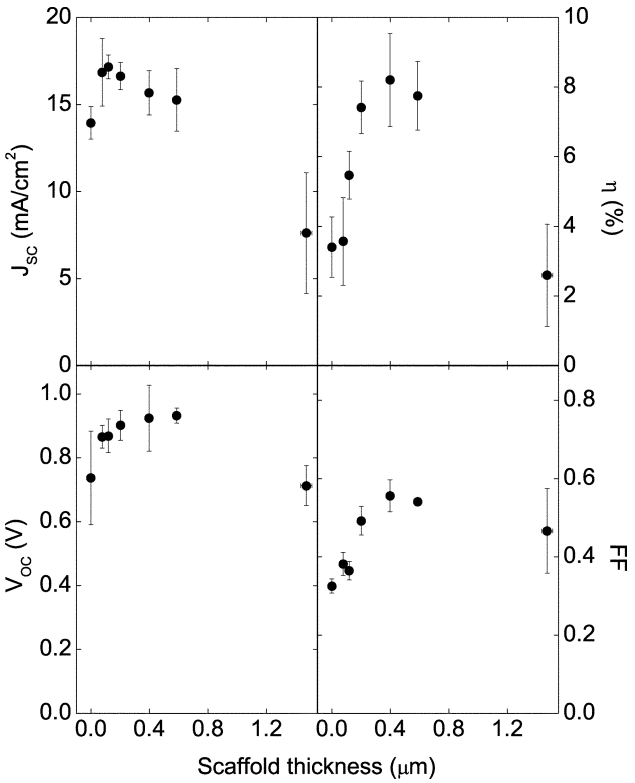

Fig. 2 Scaffold-thickness dependence of the parameters extracted from current–voltage measurements of solar cells under simulated AM 1.5, 100 mW cm^{-2} irradiance.

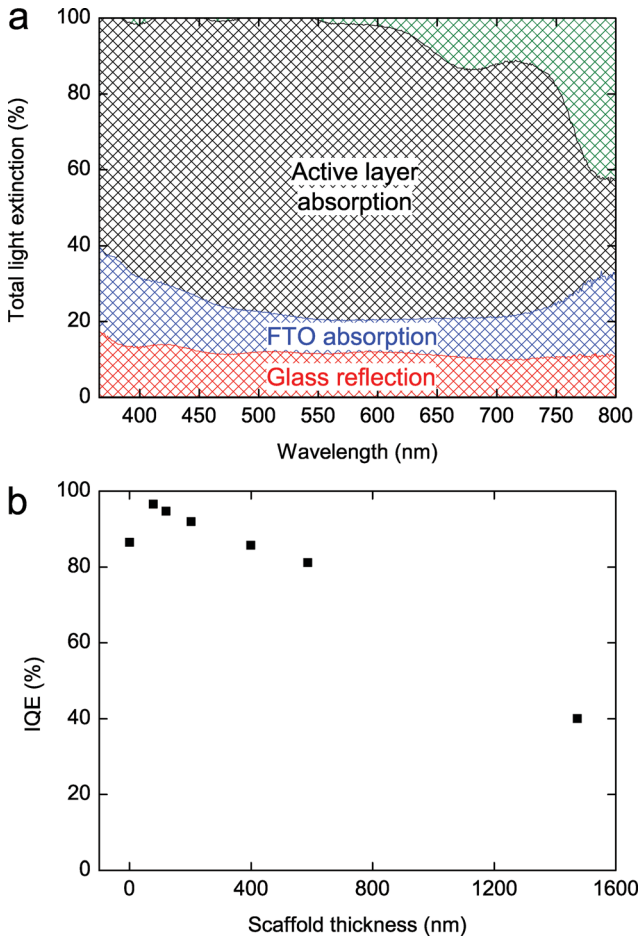

Fig. 3 Light-harvesting and internal quantum efficiency in perovskite solar cells. (a) Cumulative light extinction (absorption + reflection) through the device layers with a ~400 nm scaffold. The green region represents light which isn't collected. (b) Internal quantum efficiency integrated over the absorption spectrum as a function of scaffold thickness.

quantum efficiency (IQE). It is clear from Fig. 3b, that the increase in J_{sc} corresponds to an increase in the IQE with reducing alumina thickness. We note that the IQE here is wavelength averaged, estimated from the short-circuit current density under full sun illumination and not from external quantum efficiency measurements.

The implication of the trend in J_{sc} is highly significant. The perovskite absorber used is close in structure to $CH_3NH_3PbI_3$. The exciton binding energy in $CH_3NH_3PbI_3$ has been measured to be ~50 meV,[23] indicative of Wannier–Mott exciton formation. Hence the predominantly spontaneous dissociation of the photoinduced electron–hole pairs at room temperature is justified. However, the effective transport and collection of both the electron and holes throughout hundreds of nanometres thickness of the absorber layer is not necessarily expected. We previously observed efficient hole-transfer from the perovskite to the organic HTM,[17] and assumed that this was required to enable suitably long lived species and hence diffusion lengths for both electrons and holes in spatially separated phases (electrons in the perovskite, holes in the organic HTM), mirroring the functionality of dye-sensitized and organic bulk

heterojunction solar cells.[24–26] It has also been demonstrated that a similar perovskite can sustain long range hole transport and collection, but with the electron being transferred to mesoporous TiO_2.[16] Here, the devices exhibiting near 100% IQE are predominantly composed of solid perovskite films, indicating for the first time that a solid thin-film of the highly crystalline perovskite is both capable of ambipolar charge collection and preferable to the mesostructured composites. We observe that the crystal size in the as formed perovskite films reduces from >500 nm (precise estimation limited by the machine broadening of the X-ray diffractometer) in the solid-films, to less than 100 nm when entirely within the mesoporous alumina scaffold (see Fig. S3†). Charge trapping and recombination at the grain boundaries may therefore be responsible for the observed drop in photocurrent for the mesostructured devices.

However, in contrast to the J_{sc}, both the fill factor (FF) and open-circuit voltage (V_{oc}) initially increase with increasing scaffold thickness, peaking at ~400 nm, followed by a decrease. The initial increase in V_{oc} and FF with increasing alumina thickness is likely to emerge from a number of effects. We speculate that the alumina is acting as a buffer layer inhibiting leakage current between the electrodes.[27] In addition, it may be improving the uniform coating of the perovskite upon the substrate as is evidenced by increasing light-harvesting efficiency with increasing scaffold thickness (see Fig. S6†). The improved thin-film formation is likely to reduce the occurrence of pin-holes and "shunting paths", where, for instance, direct contact of the organic HTM with the TiO_2 compact layer would lead to enhanced dark current leakage.[28] However, further increasing the thickness beyond 400 nm decreases the FF, V_{oc} and J_{sc}, because of the increasing competition of recombination with charge collection. The power conversion efficiency, $\eta = J_{sc}V_{oc}FF/P_{in}$, where P_{in} is the incident solar power, therefore peaks at a scaffold thickness of ~400 nm.

The current–voltage curve for the highest performing solar cell, corresponding to a scaffold thickness of ~400 nm, is shown in Fig. 4. The power conversion efficiency of this device was 12.3% which is superior to that of the best reported efficiency for the high-temperature processed MSSC,[17] and matches the highest reported efficiency for liquid electrolyte DSSCs.[9] A histogram of efficiencies for identically fabricated cells is given in Fig. S7.† Devices with the low-temperature processed Al_2O_3 show much improved reproducibility, with the average efficiency increased to ~9% compared to ~6% in the previous MSSC report.[17] This clearly demonstrates that high temperature sintering of the scaffold is superfluous as a result of it serving no electronic purpose, massively increasing both the versatility and ease of manufacture of the perovskite-based solar cells. This study strongly leans towards a highly crystalline thin-film perovskite architecture ultimately leading to the highest performances once issues associated with FF and V_{oc} losses can be addressed.

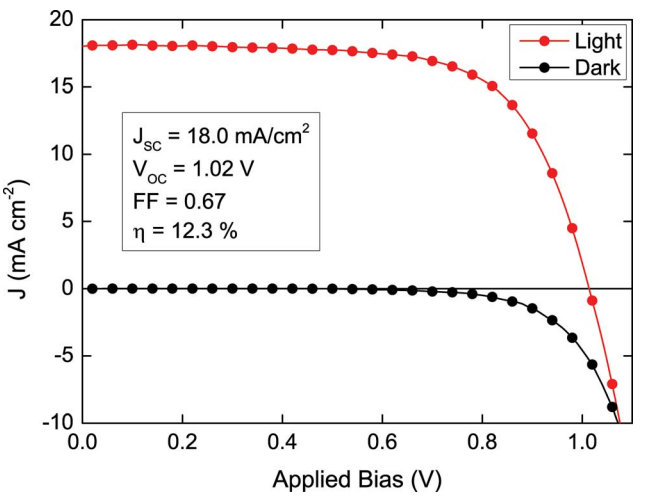

Fig. 4 Current–voltage characteristics under simulated AM 1.5, 100 mW cm^{-2} solar irradiation of the best performing ($\eta = 12.3\%$) solar cell based on a scaffold fabricated from a binder-free paste processed at temperatures not exceeding 150 °C. Solar cell performance parameters are given in the inset.

Conclusions

In summary, we have demonstrated for the first time, a solution-processable absorber that can be processed at low temperature (sub 150 °C) and efficiently fulfil the three primary functions for solar cell operation: light absorption, free charge generation, and efficient transport of both holes and electrons with minimal recombination losses in a solid thin film. This approach removes the necessity in solution-processed photovoltaics for a bulk heterojunction; separate electron and hole charge-transport media within an interpenetrating composite, greatly simplifying the device architecture. In addition, we have found that the metal oxide scaffold on which the perovskite is formed can be fabricated at low-temperature. With this approach we have achieved a remarkable power conversion efficiency of 12.3%. This renders the perovskite solar cells compatible with flexible substrates and multijunction device architectures, the latter which can lead to a further step increase in the solar cell efficiency.

Acknowledgements

This work was funded by EPSRC, the European Commission, under the SANS project (grant agreement number 246124), and ERC StG HYPER (project reference 279881). We would like to thank Ed Crossland for discussions and experimental assistance.

Notes and references

1 A. V. Shah, H. Schade, M. Vanecek, J. Meier, E. Vallat-Sauvain, N. Wyrsch, U. Kroll, C. Droz and J. Bailat, *Prog. Photovoltaics*, 2004, **12**, 113–142.
2 X. Wu, *Sol. Energy*, 2004, **77**, 803–814.
3 D. A. R. Barkhouse, O. Gunawan, T. Gokmen, T. K. Todorov and D. B. Mitzi, *Prog. Photovoltaics*, 2012, **20**, 6–11.
4 A. Chirilă, S. Buecheler, F. Pianezzi, P. Bloesch, C. Gretener, A. R. Uhl, C. Fella, L. Kranz, J. Perrenoud, S. Seyrling, R. Verma, S. Nishiwaki, Y. E. Romanyuk, G. Bilger and A. N. Tiwari, *Nat. Mater.*, 2011, **10**, 857–861.

5 C. J. Hibberd, E. Chassaing, W. Liu, D. B. Mitzi, D. Lincot and A. N. Tiwari, *Prog. Photovoltaics*, 2010, **18**, 434–452.
6 M. Graetzel, R. A. J. Janssen, D. B. Mitzi and E. H. Sargent, *Nature*, 2012, **488**, 304–312.
7 V. Fthenakis, *Renewable Sustainable Energy Rev.*, 2009, **13**, 2746–2750.
8 E. H. Sargent, *Nat. Photonics*, 2012, **6**, 133–135.
9 A. Yella, H.-W. Lee, H. N. Tsao, C. Yi, A. K. Chandiran, M. K. Nazeeruddin, E. W.-G. Diau, C.-Y. Yeh, S. M. Zakeeruddin and M. Grätzel, *Science*, 2011, **334**, 629–634.
10 Y. Liang, Z. Xu, J. Xia, S.-T. Tsai, Y. Wu, G. Li, C. Ray and L. Yu, *Adv. Mater.*, 2010, **22**, E135–E138.
11 R. F. Service, *Science*, 2011, **332**, 293.
12 J.-H. Im, C.-R. Lee, J.-W. Lee, S.-W. Park and N.-G. Park, *Nanoscale*, 2011, **3**, 4088–4093.
13 H.-S. Kim, C.-R. Lee, J.-H. Im, K.-B. Lee, T. Moehl, A. Marchioro, S.-J. Moon, R. Humphry-Baker, J.-H. Yum, J. E. Moser, M. Gratzel and N.-G. Park, *Sci. Rep.*, 2012, **2**, 591.
14 A. Kojima, K. Teshima, Y. Shirai and T. Miyasaka, *J. Am. Chem. Soc.*, 2009, **131**, 6050–6051.
15 I. Chung, B. Lee, J. He, R. P. H. Chang and M. G. Kanatzidis, *Nature*, 2012, **485**, 486–489.
16 L. Etgar, P. Gao, Z. Xue, Q. Peng, A. K. Chandiran, B. Liu, M. K. Nazeeruddin and M. Grätzel, *J. Am. Chem. Soc.*, 2012, **134**, 17396–17399.
17 M. M. Lee, J. Teuscher, T. Miyasaka, T. N. Murakami and H. J. Snaith, *Science*, 2012, **338**, 643–647.
18 Z. M. Beiley and M. D. McGehee, *Energy Environ. Sci.*, 2012, **5**, 9173–9179.
19 P. Zhang, C. Wu, Y. Han, T. Jin, B. Chi, J. Pu and L. Jian, *J. Am.Ceram. Soc.*, 2012, **95**, 1372–1377.
20 T. Miyasaka, M. Ikegami and Y. Kijitori, *J. Electrochem. Soc.*, 2007, **154**, A455–A461.
21 C. Y. Jiang, W. L. Koh, M. Y. Leung, S. Y. Chiam, J. S. Wu and J. Zhang, *Appl. Phys. Lett.*, 2012, **100**, 113901.
22 E. J. W. Crossland, N. Noel, V. Sivaram, T. Leijtens, J. A. Alexander-Webber and H. J. Snaith, *Nature*, 2013, **495**, 215–219.
23 K. Tanaka, T. Takahashi, T. Ban, T. Kondo, K. Uchida and N. Miura, *Solid State Commun.*, 2003, **127**, 619–623.
24 J. J. M. Halls, C. A. Walsh, N. C. Greenham, E. A. Marseglia, R. H. Friend, S. C. Moratti and A. B. Holmes, *Nature*, 1995, **376**, 498–500.
25 G. Yu, J. Gao, J. C. Hummelen, F. Wudl and A. J. Heeger, *Science*, 1995, **270**, 1789–1791.
26 B. O'Regan and M. Gratzel, *Nature*, 1991, **353**, 737–740.
27 P. Docampo and H. J. Snaith, *Nanotechnology*, 2011, **22**, 225403.
28 H. J. Snaith, N. C. Greenham and R. H. Friend, *Adv. Mater.*, 2004, **16**, 1640–1645.